Engineering Structures 327 (2025) 119637

Contents lists available at ScienceDirect

Engineering Structures

journal homepage: www.elsevier.com/locate/engstruct

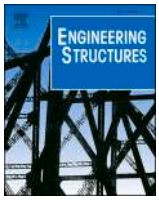

Study on active control for multilinear and nonlinear vibration in piezoelectric structures through a secondary channel improved method

Xudong Zhang [a], Xin Lan [b], Weikai Shi [a], Pengxiang Zhao [a], Jianlong Gao [a], Liwu Liu [a,*], Yanju Liu [a,*], Jinsong Leng [b]

[a] Department of Astronautical Science and Mechanics, Harbin Institute of Technology, Harbin 150001, China
[b] Centre for Composite Materials and Structures, Harbin Institute of Technology, Harbin 150080, China

ARTICLE INFO

Keywords:
RU-FxLMS controller
Active vibration control
Multiline spectra
Narrowband spectra
Piezoelectric structures

ABSTRACT

Focusing on multiline and narrowband spectral vibration control issues presented by engineering requirements, this study assessed the effectiveness of large-scale and high-rigidity structures equipped with piezoelectric stack actuators for the active control of vibration. By utilizing the modal decomposition approach, the derivation yielded a state-space equation for an Nth-order system of a piezoelectric cantilever beam was deduced. On this foundation, the traditional least mean square algorithm was improved, and a resettable uniformization filtered-x least mean square (RU-FxLMS) controller was designed, which effectively mitigated the adverse effects of filtering and prevented beating vibration phenomena during the control process. This improvement has, to a certain extent, compensated the deficiencies of the adaptive strategy over low frequency line spectral vibration. Afterwards, Simulations and experimental pertaining to active vibration control of piezoelectric cantilever beams were performed. Experimental data, gathered under the conditions of multiline spectra, narrowband spectra, and frequency-hopping vibration, exhibited a relatively obvious control effect. Under two typical vibration conditions, the simulations and experiments exhibited reasonable and consistent control trends at each characteristic line spectrum, which validated the feasibility and reliability of this strategy for vibration control in the low frequency domain with piezoelectric structures.

1. Introduction

The vibration characteristics of engineering structures play a role in determining the performance of equipment and facilities and have significant theoretical implications and engineering value. Currently, structural vibration serves as a crucial index for assessing the reliability of structures and systems. In the realm of vibration engineering, there exists no universally standardized demarcation for frequency ranges. Typically, low frequency vibration are characterized by frequencies ranging from 0 to 100 Hz and are commonly observed in large-scale structures such as buildings. Conversely, high frequency vibration are generally defined as those exceeding 1 kHz and are frequently encountered in smaller structural components, such as mechanical parts. Passive vibration control methods, which were initially developed to primarily target the attenuation of medium-high frequency structural vibration, exhibit limited efficacy in controlling low frequency line spectra and narrowband vibration. With the accelerated advancement of and combination of smart materials and structures with control science and engineering, active control of structural vibration utilizing smart materials has emerged as a burgeoning research focus. Piezoelectric materials, owing to their intelligent characteristics, lightweight nature, and superior linearity, have garnered relatively extensive utilization in the domain of active vibration control.

With the development and application of smart materials in the field of vibration control, numerous studies provided novel insights. Devices such as piezoelectric ceramic transducer (PZT) [1,2] and macro fiber composite (MFC) [3–6] were employed as actuators and sensors in vibration control applications. Previous studies employed optimization algorithms, including genetic algorithms and non-dominated sorting genetic algorithm-II (NSGA-II), to meticulously optimize the positions and parameters of piezoelectric actuators [7–9]. Additionally, optimization designs for sensors were implemented [10,11], and the integration of piezoelectric devices was pursued [12]. Traditional vibration control strategies were also extensively studied in the field, encompassing the use of infinity norm controllers [13] and linear quadratic regulators (LQR) observers [14–17] within robust control theory frameworks, which provided effective mathematical solutions for

* Corresponding authors.
E-mail addresses: liulw@hit.edu.cn (L. Liu), yj_liu@hit.edu.cn (Y. Liu).

https://doi.org/10.1016/j.engstruct.2025.119637
Received 26 August 2024; Received in revised form 13 December 2024; Accepted 2 January 2025
Available online 16 January 2025

Nomenclature

RU-FxLMS	Resettable uniformization filtered-x least mean square
LSF	Line spectral frequency
$\varphi_i(x)$	The ith-order mode shape function
x_s	The control point coordinates
x_e	The observation point coordinates
m_i	The ith-order modal mass
ω_{ni}	The ith-order natural frequency
ζ_i	The ith-order damping ratio
d_{ij}	The piezoelectric strain constant
D_i	The potential shift
s_{ij}^E	The elastic modulus at a constant electric field strength
ε_{ij}^σ	The dielectric constant at a constant external stress
E_i	The electric field strength
n	The number of stacking layers
A	The cross-sectional area
h	The thickness of stacking layers
h_s	The actuating distance
u_c	The control input in the system
μ	The convergence step
$x(k)$	The reference signal
$P(z)$	The transfer function of the signal transmission path
$C(z)$	The transfer function of the secondary channel
$C'(z)$	The estimation of the transfer function of the secondary channel
$d(k)$	The vibration signal received by the displacement sensor
$y(k)$	The controller output signal after algorithm iteration
$s(k)$	The feedback signal
$W(z)$	The LMS adaptive filter
$r(k)$	The filtered signal
$h(k)$	The output signal of the RU-FxLMS

vibration control in complex systems. proportional-integral-derivative (PID) controllers [18–20], infinite impulse response (IIR) filter-based least mean square (LMS) controllers [21–23], LQR [24], auxiliary stochastic noise methods [25], and radial basis function (RBF) neural network feedforward controllers [26,27] were employed to optimize signal processing, thereby enhancing the stability and response speed of control systems. In the realm of non-traditional vibration control strategies, adaptive control remained a longstanding research focus, capable of real-time adjustment and optimization of system dynamics to address nonlinear issues [28–30]. The model predictive control (MPC) method enhanced its adaptability to complex vibration environments through real-time optimization and prediction of system dynamics. Research indicated that the MPC method effectively suppressed vibrations and improved control performance, particularly excelling in nonlinear and multivariable systems [31–33]. Furthermore, the combination of MPC with other advanced algorithms further enhanced its robustness and real-time performance, providing a novel solution for structural vibration control. Meng et al. [34] proposed a multi-input multi-output multi-harmonic feedforward adaptive control method utilizing piezoelectric stack actuators, which significantly reduced the vibration levels of helicopter fuselages. Xie et al. [35] proposed a fractional order PD control method for lattice grid beams based on piezoelectric fiber composite panels, which can significantly and rapidly reduce the vibration amplitude of lattice grid beams. Several studies developed new control laws or parameter models, proposing novel approaches to optimize system performance under specific conditions while maintaining system stability and optimizing other performance indices [36–38]. Research on topology optimization of piezoelectric structures has also emerged as a significant focus area. Zhang et al. employed finite element analysis and sensitivity analysis using the adjoint variable method [39,40], effective reductions in energy consumption under harmonic excitations were achieved, leading to enhanced control performance. Furthermore, existing research has also applied control methods to various practical scenarios, including submerged systems [41], annular antenna structures [42], shape memory polymer composites [43], and buildings [44–46]. In large-scale and high-rigidity structures within engineering applications, the emergence of multiline spectra and narrowband spectra vibration at low frequency is a frequent occurrence. The implementation of active control strategies can significantly enhance the vibration damping effectiveness of these structures within the low frequency range. Building upon previous research, this paper proposed an improved algorithm based on the filtered-x least mean square (FxLMS) algorithm, derived the constitutive control model for piezoelectric cantilever beams, and conducted simulations and experimental validations of multiline spectra and narrowband spectra vibration active control under multiple operating conditions on a large-section steel structure piezoelectric beam. Consistency comparisons between control simulations and experimental results were performed under typical operating conditions. Additionally, we compared the improved algorithm with traditional algorithms under the same operating conditions and analyzed the advantages of the improved algorithm, which partially improved the deficiencies of the adaptive method regarding line spectrum responses. This study employed a structure characterized by a large stiffness and size cantilever beam, combined with embedded piezoelectric materials for vibration control research, aiming to provide a reference for the research on linear and nonlinear vibration control of low frequency structures in engineering.

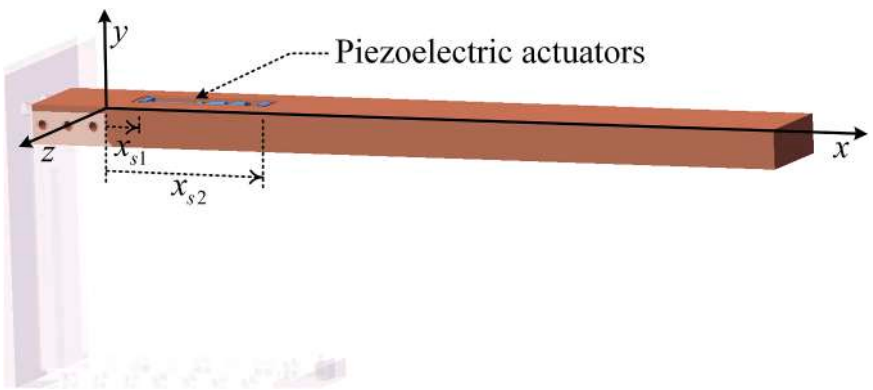

Fig. 1. Schematic of the piezoelectric cantilever beam.

2. Cantilever beam theory with piezoelectric actuators

2.1. Constitutive equations

Cantilever beams are fundamental structures commonly encountered in engineering. This study investigates the active vibration control capabilities of piezoelectric structures with a focus on cantilever beams under conditions such as online spectra and narrowband vibration. The schematic of the piezoelectric cantilever beam is presented in Fig. 1.

Given the utilization of a high-stiffness cantilever beam, the displacement and deformation were relatively small during vibration, thus allowing the nonlinear behavior associated with large deformations to be neglected. The constitutive equations for the cantilever beam were modeled based on the Euler-Bernoulli beam assumption. The differential equations governing the transverse vibration of a uniform beam subjected to an external disturbance force are as follows:

$$m\frac{\partial^2 y}{\partial t^2}+c\frac{\partial y}{\partial t}+EI\frac{\partial^4 y}{\partial x^4}=f\left(x,t\right) \tag{1}$$

When the excitation is a transverse force, the external force is expressed as

$$f(x,t)=F(t)\delta(x-x_1) \tag{2}$$

By utilizing the principle of modal orthogonality, the transfer function at any point on the beam can be readily derived.

$$G_i(s)=\frac{\varphi_i(x_s)\varphi_i(x_e)}{m_i\left(s^2+2\zeta_i\omega_{ni}s+\omega_{ni}^2\right)} \tag{3}$$

where x_s is the input point, x_e is the output point, m_i is the ith-order modal mass, extending to a state space of order N, the state-space equation can be formulated as

$$\begin{cases} x'_1=x_2 \\ x'_2=-\omega_{n1}^2x_1-2\zeta_1\omega_{n1}x_2+\dfrac{\varphi_1(x_s)}{m_1}u \\ \cdots \\ x'_{2N-1}=x_{2N} \\ x'_{2N}=-\omega_{nN}^2x_{2N-1}-2\zeta_N\omega_{nN}x_{2N}+\dfrac{\varphi_N(x_s)}{m_N}u \end{cases} \tag{4}$$

$$y=\varphi_1(x_e)x_1+\varphi_2(x_e)x_3+\cdots+\varphi_N(x_e)x_{2N-1}$$

The system matrix is

$$A=\begin{bmatrix} 0 & 1 & & & \\ -\omega_{n1}^2 & -2\zeta_1\omega_{n1} & & & \\ & & \cdots & & \\ & & & 0 & 1 \\ & & & -\omega_{nN}^2 & -2\zeta_N\omega_{nN} \end{bmatrix}_{2N\times 2N} \tag{5}$$

The input matrix $B=\left[0,\frac{\varphi_1(x_s)}{m_1},\cdots,0,\frac{\varphi_N(x_s)}{m_N}\right]^T_{2N\times 1}$

If the excitation defined by Eq. (2) is expressed in a bending moment form, then

$$f\left(x,t\right)=M_0\frac{\partial}{\partial x}[\delta(x-x_2)-\delta(x-x_1)] \tag{6}$$

Correspondingly, the transfer function will be the same at any point on the beam:

$$G_i(s)=\frac{[\varphi'_i(x_{s2})-\varphi'_i(x_{s1})]\varphi_i(x_e)}{m_i\left(s^2+2\zeta_i\omega_{ni}s+\omega_{ni}^2\right)} \tag{7}$$

Extending this to a system of order N, the state-space equation can be formulated as

$$\begin{cases} x'_1=x_2 \\ x'_2=-\omega_{n1}^2x_1-2\zeta_1\omega_{n1}x_2+\dfrac{[\varphi'_1(x_{s2})-\varphi'_1(x_{s1})]}{m_1}u \\ \cdots \\ x'_{2N-1}=x_{2N} \\ x'_{2N}=-\omega_{nN}^2x_{2N-1}-2\zeta_N\omega_{nN}x_{2N}+\dfrac{[\varphi'_N(x_{s2})-\varphi'_N(x_{s1})]}{m_N}u \end{cases} \tag{8}$$

$$y=\varphi_1(x_e)x_1+\varphi_2(x_e)x_3+\cdots+\varphi_N(x_e)x_{2N-1}$$

At this point, the system input matrix is$B=\left[0,\frac{[\varphi'_1(x_{s2})-\varphi'_1(x_{s1})]}{m_1},\ldots,0,\frac{[\varphi'_N(x_{s2})-\varphi'_N(x_{s1})]}{m_N}\right]^T_{2N\times 1}$

The operating frequency range of the ceramics was significantly lower than their resonant frequency, thus the dependence of the piezoelectric constant on frequency was neglected. The constitutive equations for the piezoelectric stacked ceramics were modeled based on the linear elasticity assumption, homogeneity assumption, small displacement assumption, and the assumption of negligible interfacial effects, etc. Due to the thin and brittle nature of a piezoelectric ceramic sheet, the additional bending moments resulting from its attachment to a structure are considered negligible. If the d_{33} effect only occurs in the polarization thickness direction, then the one-dimensional piezoelectric equation in the axial direction is

$$\begin{cases} \varepsilon_3=s_{33}^E\sigma_3+d_{33}E_3 \\ D_3=d_{33}\sigma_3+\varepsilon_{33}^\sigma E_3 \end{cases} \tag{9}$$

where ε_3 represents the axial strain, D_3 represents the axial potential shift, σ_3 represents the axial stress, s_{33}^E represents the axial elastic modulus at a constant electric field strength, ε_{33}^σ represents the dielectric constant at a constant external stress, d_{33} represents the piezoelectric constant, and E_3 represents the electric field strength. When there is no constraint on the polarization direction of the piezoelectric ceramic and the effect of external excitation is neglected, the strain equation is linear. If the number of laminated sheets is n, the area is A, the thickness in the polarization direction of each sheet is h, and the strain deformation of

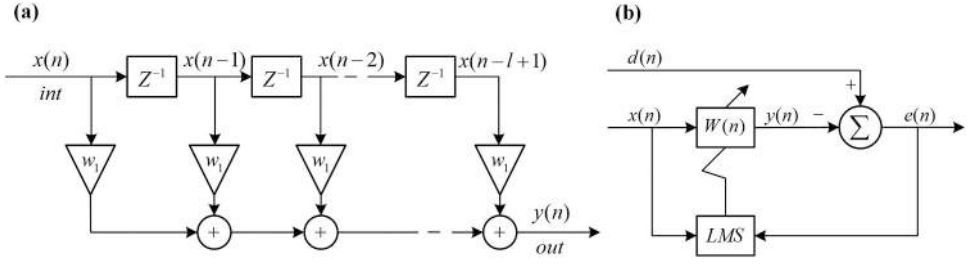

Fig. 2. (a) Block diagram of the lateral adaptive filter structure, (b) Block diagram of the adaptive LMS algorithm filter system.

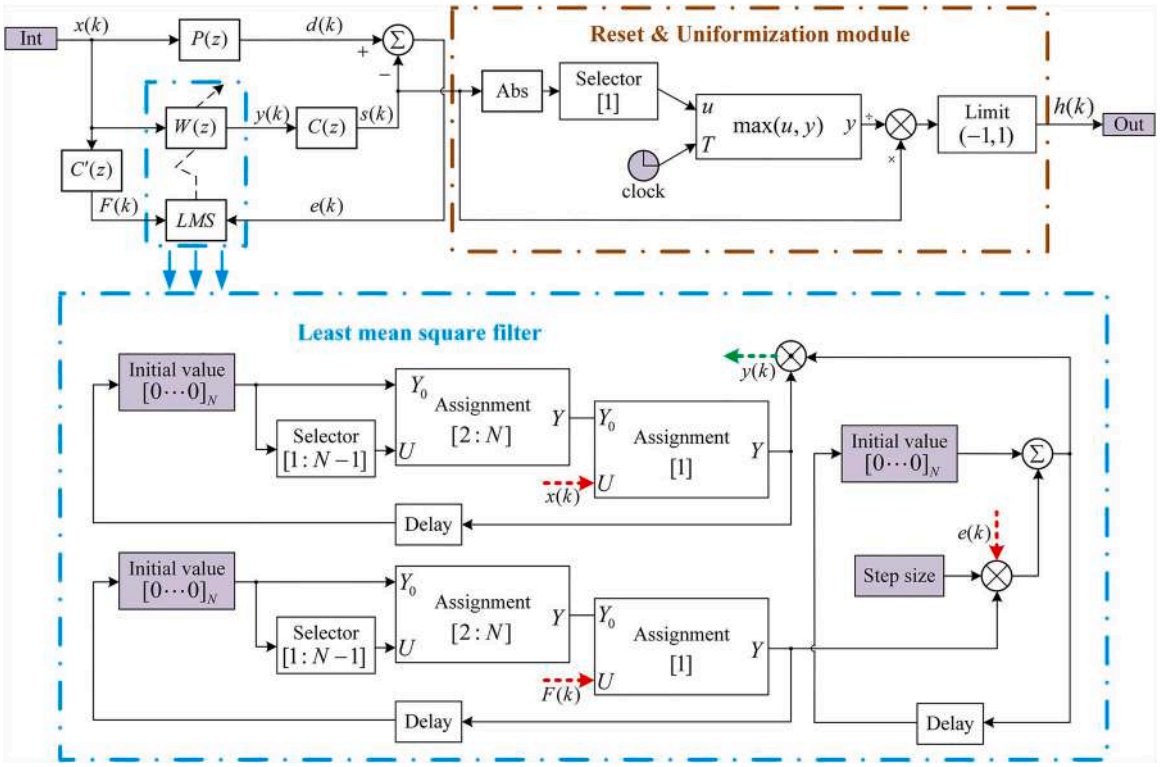

Fig. 3. Block diagram of the RU-FxLMS algorithm.

the piezoelectric sheet in the polarization direction under the action of an applied alternating voltage $U(t)$ is δ, then the electrostatic strain $\varepsilon = \delta/h$. Under no-load conditions, a single piezoelectric ceramic is subjected to the following stress:

$$\sigma_3 = c_{33}^E\left(\varepsilon_3 - \frac{\delta}{h}\right) \tag{10}$$

Consequently, within a piezoelectric cantilever structure composed of stacked ceramic layers, the control force can be modified according to Eq. (6).

$$\begin{aligned} f\left(x,t\right) &= \frac{nh_s d_{33} UA}{s_{33}^E nh}\frac{\partial}{\partial x}\left[\delta(x-x_2)-\delta(x-x_1)\right] \\ &= u_c\frac{\partial}{\partial x}\left[\delta(x-x_2)-\delta(x-x_1)\right] \end{aligned} \tag{11}$$

where h_s signifies the distance from the axis of the piezoelectric ceramic to the neutral axis of the cantilever beam and u_c is the control input in the system.

2.2. Governing equations

The basis of the active control system lies in the design of the controller, which includes both filter and algorithmic components. The algorithm adaptively adjusts the filter coefficients to facilitate the filtering process. Fig. 2(a) shows the configuration of the lateral adaptive filter. The LMS algorithm performs iterative operations aiming to minimize the root mean square error of the predefined target value by employing a finite impulse response structure. Fig. 2(b) displays the block diagram for the LMS algorithm filter system, where $d(n)$ and $e(n)$ are used in the control system as target and error signals.

The root mean square of the error signal at time n is

$$J(n) = E\left[e^2(n)\right] = E\left[\left(d(n)-y(n)\right)^2\right] \tag{12}$$

The gradient is determined by differentiating Eq. (12) to achieve the minimum root mean square error of the signal.

$$\nabla(n) = \left.\frac{\partial J(n)}{\partial W}\right|_{W=W(n)} = \left[\frac{\partial J(n)}{\partial w_1}, \frac{\partial J(n)}{\partial w_2}, \cdots, \frac{\partial J(n)}{\partial w_L}\right] \tag{13}$$

The gradient $\nabla(n)$ of the squared error signal for unbiased estimation is taken in the LMS algorithm, yielding the following result:

$$\widehat{\nabla} = \frac{\partial e^2(n)}{\partial W} = -2e(n)X(n) \tag{14}$$

In accordance with the steepest descent theory principles, setting the Eq.(13) to zero and combine Eq.(14) allows the expression of the filter weight vector $W(n+1)$ at the subsequent instant to be obtained, where μ is the convergence step. This is a consequence of determining the filter coefficient W_0 at the instance of the minimum error signal.

$$W(n+1) = W(n) + 2\mu e(n)X(n) \tag{15}$$

The algorithm used in the active vibration control system in this study is illustrated in Fig. 3, where $x(k)$ represents the reference signal, $P(z)$ represents the transfer function between the two endpoints of the signal transmission path, $C(z)$ represents the transfer function of the secondary channel, $C'(z)$ represents the estimation of the equivalent transfer function of the secondary channel, $d(k)$ represents the vibration signal received by the displacement sensor, $y(k)$ represents the controller output signal after algorithm iteration, and $s(k)$ represents the feedback signal after $C(z)$ and $e(k)$ is the system error signal. $W(z)$ represents the LMS adaptive filter.

In the vibration control experiments, two related factors affecting the control efficacy were identified: the inherent time delay of the physical channels and the proportion of high frequency components in the error signals picked up by the sensors. Compensating for time delays through feedback compensation is subject to certain limitations, which may potentially lead to stability issues within the system. Consequently, a feedforward approach is commonly employed to mitigate these delay effects. Focusing on the second influencing factor, the resettable uniformization filtered-x least mean square (RU-FxLMS) control strategy proposed herein was grounded in adaptive filtering algorithms, which

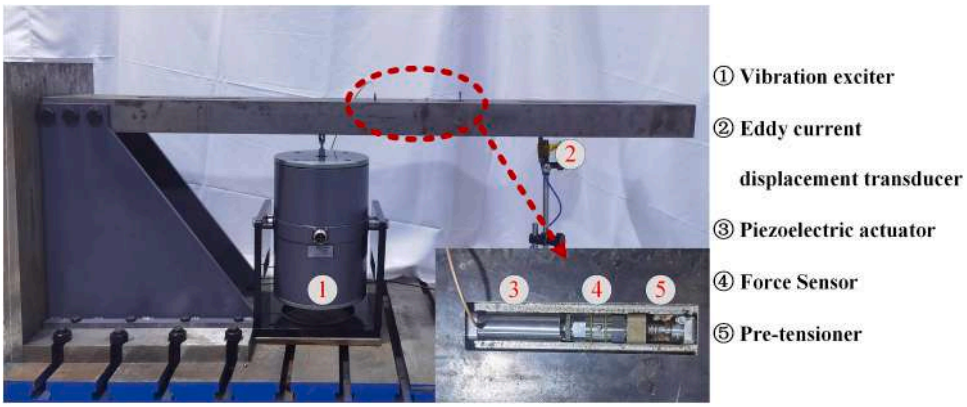

Fig. 4. Active vibration control platform for high-rigidity cantilever beams.

facilitated continuous low-pass filtering within the closed-loop computations and enabled online identification of the secondary channels to augment control efficacy. Additionally, during the algorithm execution, the signal $s(k)$ amplitude is reset and compensated at each fixed step to ensure that the input signal to the driver remains smooth and that the output capability is maximized. The feedback signal was subjected to reset and uniformization processing before acquisition, thereby mitigating the detrimental impacts of filtering and preventing the beat phenomena during the control procedure, which compensated for the shortcomings in adaptive control over low frequency line spectra to a certain extent.

The signal propagation through a channel is characterized by a convolution of the signal with the channel transfer function. The output of the RU-FxLMS algorithm is presented for a filter of order L and a moment length of k.

$$y(k) = X^T(k)W(k) = W^T(k)F(k) = \sum_{l=1}^{L} w_l(k)f(k-L+1) \tag{16}$$

Then, we obtain

$$s(k) = \sum_{l=1}^{L} w_l(k)r(k-L+1) = r^T(k)W(k) \tag{17}$$

where $r(k)$ denotes the convolution of the reference signal with the transfer function of the secondary channel.

$$e(k) = d(k) + s(k) = d(k) + r^T(k)W(k) \tag{18}$$

A parallel derivation yields a relationship for the filter weights, which is expressed as follows:

$$W(k+1) = W(k) - 2\mu e(k)r(k) \tag{19}$$

Through the reset and uniformization module, the output signal $h(k)$ satisfies the following definitions, where A is the signal maximum amplitude, T is the number of resets, and t is the duration of each reset.

$$\forall t, k \in R, \exists A \in R; \left\{ h(k) = \frac{s(k)}{s(k_T)} \le A, \left(T-1\right)t \le k_T \le Tt | T \in Z^+ \right\} \tag{20}$$

3. Preparation

To minimize the impact of fixed boundary conditions on the results of the vibration control experiments, the cantilever beam was secured to the rib plate and L-beam using bolts. Additionally, the assembly was anchored to the cast iron platform with bolts to establish a high-rigidity active control platform for cantilever beam vibration. This configuration is depicted in Fig. 4. The cantilever beam employed was 1200 mm long, 150 mm wide, and 60 mm thick and was constructed from Q235 ordinary carbon structural steel. A shaker (model JZK-50) was vertically mounted 450 mm from the fixed end of the cantilever to induce vibration. The piezoelectric actuator, force transducer (model CL-YD-2311), and prestressing device were embedded in series at the midspan of the cantilever beam, 700 mm from the fixed end. An eddy current displacement transducer (model ZA-21) was installed 200 mm vertically above the distal end of the cantilever to measure the vibration displacements at that point.

The experiment was conducted by employing a closed-loop control method, the principle of which is illustrated in Fig. 5. The semiphysical control platform was outfitted with an 8-channel verified time controller (model PXIe-8881, equipped with a Linux RT real-time operating system), a 2-channel 24-bit analogue output dynamic signal generator (model PXIe-4463), and a 16-channel 24-bit dynamic signal acquisition

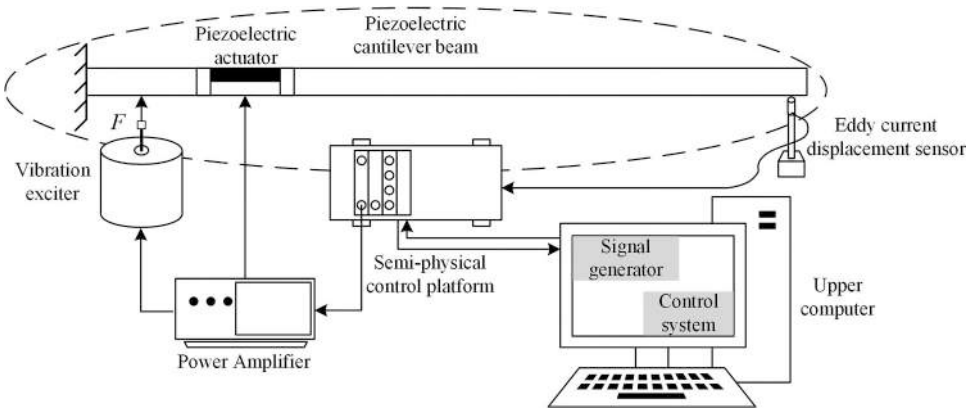

Fig. 5. Schematic diagram of the principle of closed-loop control method.

Table 1
Structural properties and boundary conditions in simulation.

Parameters	Value
Cantilever Beam Length	1.2 m
Damping Ratio	0.03
Young's modulus	$2.1e^{11}$ Pa
Sectional Moment of Inertia	$2.7e^{-6}$ m^4
First four modal masses	84.77/84.78/85.78/84.88 Kg
Linear Mass	70.65 Kg/m
Excitation input point location	0.45 m
Bending moment control point location	0.2 m
Vibration observation point location	1 m
Driver to Neutral Distance	0.0175 m
Driver length	0.07 m

card (model PXIe-4497). The control platform was interfaced with the host computer to enable real-time data exchange. The analogue signal was generated by the host computer, and the voltage signal was produced by the dynamic signal generator through a power amplifier (model YE5874A) to drive the shaker, thereby stimulating vibration of the cantilever. The eddy current displacement transducer collected vibration data and transmitted analogue signals through the dynamic signal capture card to the host computer. The control system generated real-time control signals and produced voltage signals via the dynamic signal generator, which then drove the piezoelectric actuator through a piezoelectric ceramic power amplifier (model E00. C3) to damp the oscillation of the cantilever. Data exchange was conducted in real time, and the algorithm was executed in 1 ms increments.

The FxLMS algorithm is recognized as a widely utilized adaptive control algorithm in the field of active vibration control owing to its simplicity of description and comprehension. In particular, the algorithm requires only multiplication and addition operations, aligning well with the operational structure of standard PXIe hardware. This compatibility facilitates adaptation and implementation in actual engineering application systems. After the output signal reset capability of the FxLMS algorithm was optimized, the robustness of the algorithm was further enhanced in the face of physical modelling errors and truncation errors arising from finite computational accuracy.

This manuscript focuses on active control of multiline spectra and narrowband vibration within high-rigidity piezoelectric cantilever beam structures. Initially, the response of a high-rigidity cantilever beam structure to forced vibration was investigated using the hammering method to determine the dynamic characteristics of the structure. Subsequently, closed-loop vibration control experiments were conducted on a high-rigidity piezoelectric cantilever beam structure utilizing the RU-FxLMS control algorithm, during which the vibration data of the structure were collected.

4. Results and discussion

4.1. Simulation of active control of piezoelectric cantilever vibration

The traditional FxLMS algorithm required secondary path estimation through identification. An improvement was made by incorporating an online identification method in the secondary path, enabling the accurate and real-time acquisition of the physical channel model. To establish a more accurate physical model for the secondary channels, rather than directly applying the primary channel models, necessitating the addition of an analogue filter, designated $C'(z)$, to compensate for the transfer characteristics of the secondary channel. The actual channel was replaced with an online detected model for controller computation, and random white noise was introduced as a training signal, enabling the controller to achieve better coverage of the input signal spectrum. Consequently, this approach allowed a more accurate estimation of the transfer function of the secondary channel. In modelling the mechanics of the piezoelectric cantilever beam, physical parameters such as the beam length, structural damping, Young's modulus, sectional moment of inertia, linear mass, length of the piezoelectric ceramic, distance along the central axis of the piezoelectric ceramic, neutral axis of the

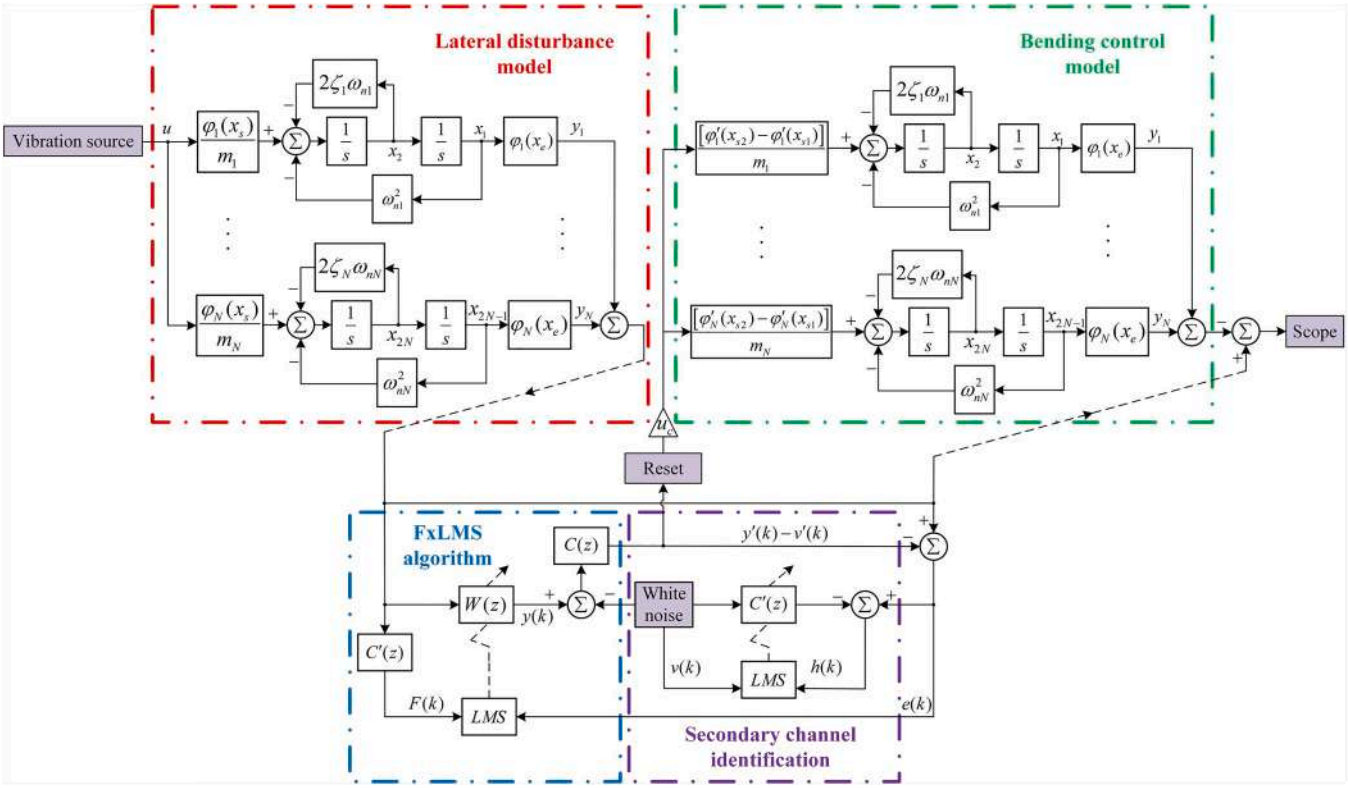

Fig. 6. Block diagram for the active control system of the cantilever beam.

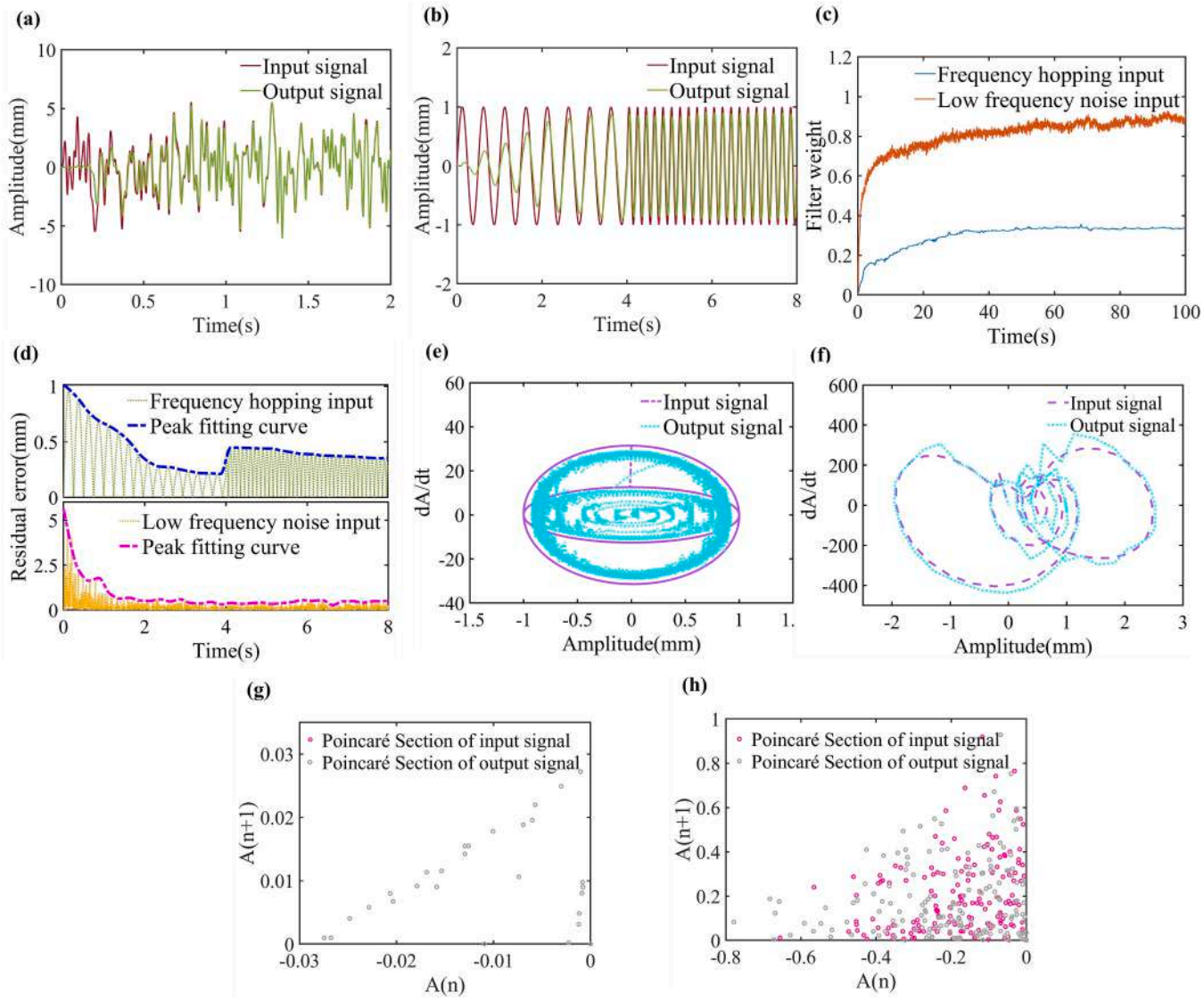

Fig. 7. Diagram of algorithm tracking and convergence effect (a) Frequency-hopping signal tracking effect, (b) Low frequency noise signal tracking effect, (c) Filter weight convergence effect, (d) Residual and fitting effect, (e) Phase trajectory diagram of frequency-hopping, (f) Phase trajectory diagram of low frequency noise, (g) Poincare map of frequency-hopping, (h) Poincare map of low frequency noise.

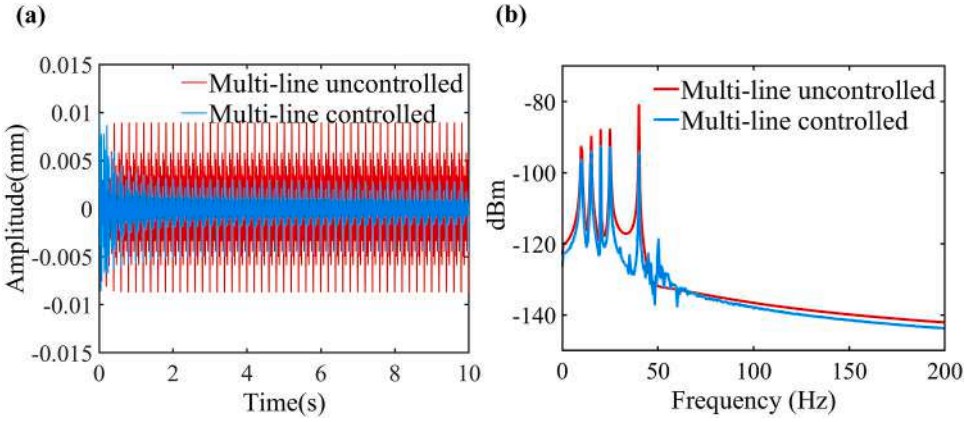

Fig. 8. Simulation results of active control of multiline spectral vibration (a) Time domain diagram before and after control, (b) Frequency domain diagram before and after control.

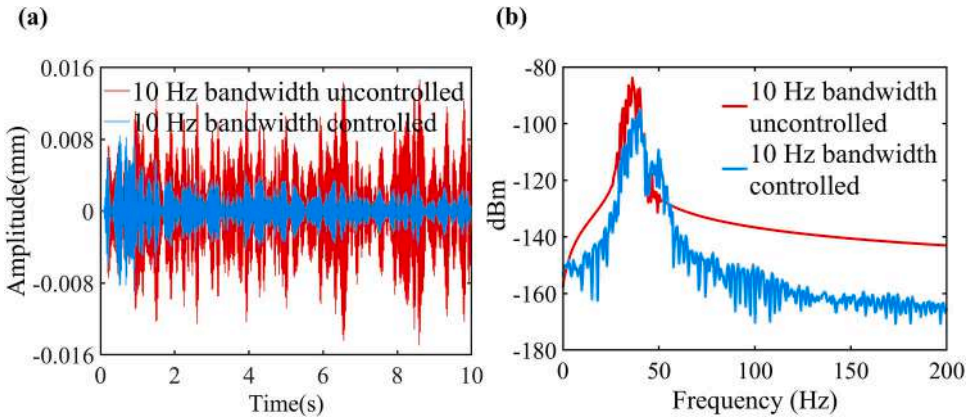

Fig. 9. Simulation results of active control of narrowband spectral vibration (a) Time domain diagram before and after control, (b) Frequency domain diagram before and after control.

beam, mounting position of the piezoelectric ceramic, position of the perturbation point, and position of the observation point were input as boundary conditions, which are illustrated in Table 1.

The disturbance force was input into the transverse vibration state-space Eq. (9) of the cantilever beam, and the vibration displacement observed at the observation point was processed using the FxLMS control algorithm. This processed displacement was subsequently fed back through the force-electric coupling characteristic of the secondary channel piezoelectric ceramic to control the bending moment exerted by the actuator. The control bending moment was then input into Eq. (14), which pertains to the state space of the cantilever beam transverse vibration, thereby completing active vibration control of the piezoelectric cantilever beam via the modal superposition method. Fig. 6 shows a block diagram of the active control system of the cantilever beam.

Prior to the simulation, the performance of the algorithm and the convergence of the filtering were verified and analysed to ensure the robustness of the truncation error under the object modelling errors and limited computational accuracy. When the control system received frequency-hopping simple harmonic signals and low frequency noise signals, the tracking performance of the output signal was satisfactory. Following the online determination of the secondary channel, the system displayed increased sensitivity to the tracking of low frequency noise signals, and a more rapid convergence of the filter weights was achieved. The tracking efficiency, convergence, and nonlinear characteristics of the algorithm were illustrated in Fig. 7.

As shown in Fig. 7(a)-(d), the improved algorithm demonstrated good tracking performance for both types of signals. It exhibited a faster convergence speed of filter weights and residuals for noisy signals and also showed improvements in the deficiencies of line spectrum response. As illustrated in Fig. 7(e)-(h), the improved algorithm exhibited a favorable response for both linear and chaotic systems. However, it required a longer computation time to achieve convergence in linear systems.

The input point of the system was set 450 mm from the root, and the external disturbance force was configured as a superimposed spectrum of simple harmonic waves with frequencies of 10, 15, 20, 25, and 40 Hz and an amplitude of 20 N. Fig. 8 displays the simulated effect of the active vibration control for the external disturbances with a multiline spectrum based on the piezoelectric cantilever beam model.

The external disturbance force applied to the system was set as Gaussian white noise with a power spectral density amplitude of 50. This resulted in a narrowband spectrum ranging between 30 Hz and 40 Hz after filtering. The simulated effect of active vibration control for the external disturbance within this narrowband spectrum, based on the piezoelectric cantilever model, is depicted in Fig. 9.

In light of the simulation results obtained, enhanced control performance was demonstrated for the piezoelectric cantilever when the RU-FxLMS control algorithm was applied for both multiline and narrowband spectra. For the disturbances characterized by multiline spectra, a suppression effect ranging from 4 to 13 dBm was achieved for

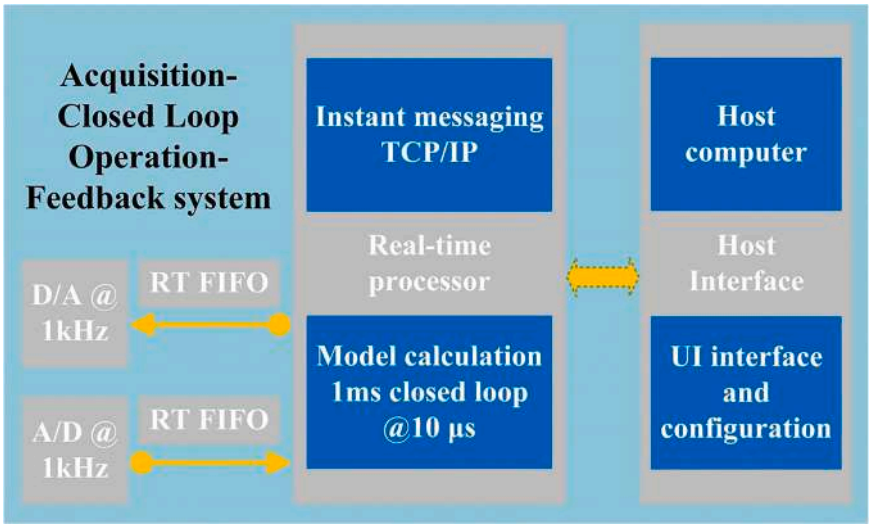

Fig. 10. The design architecture diagram of the acquisition-closed loop operation-feedback system.

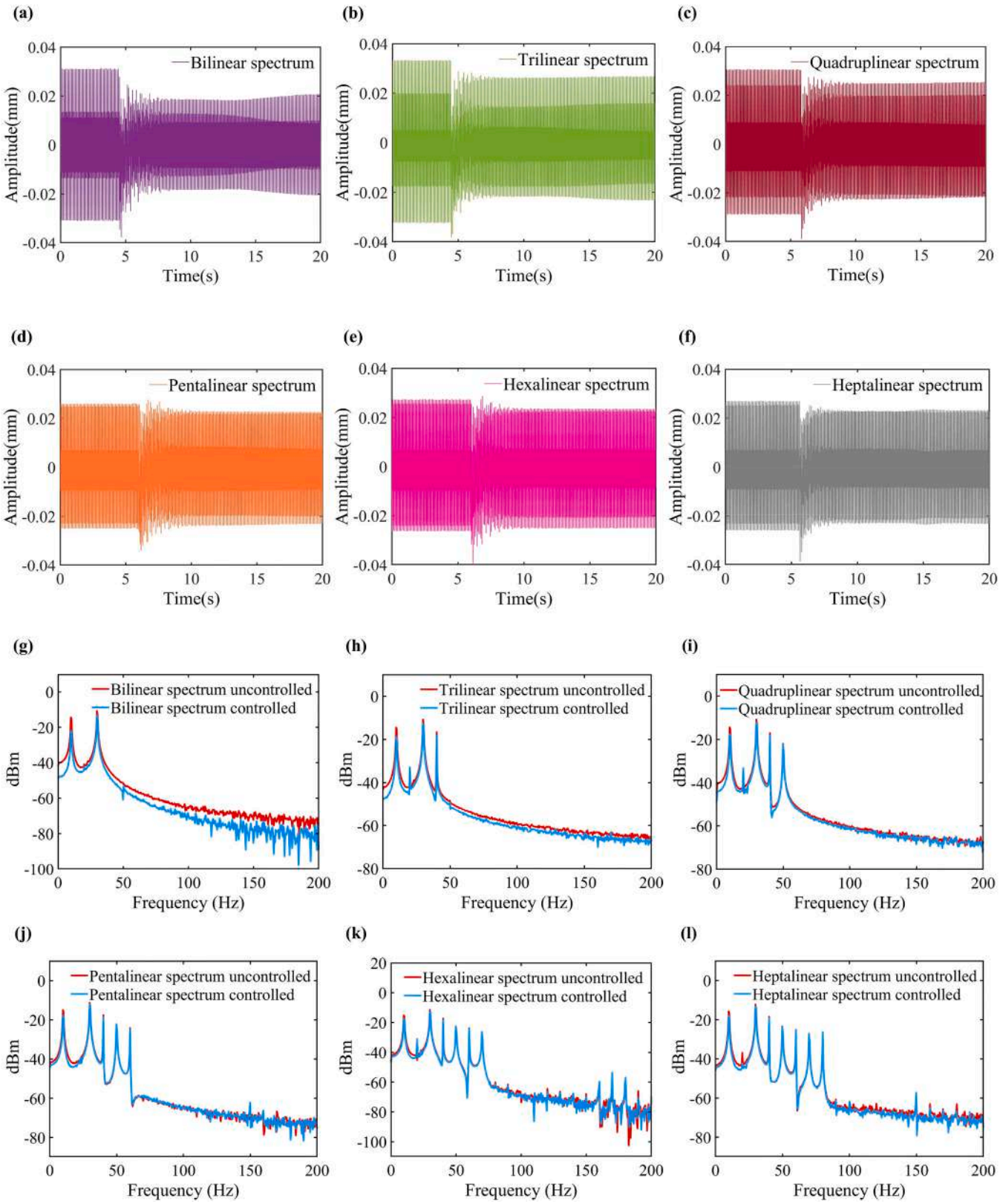

Fig. 11. Experimental results of active control of multiline spectral vibration, Fig(a) to (l) are time and frequency domain diagram before and after controlling the number of line spectra.

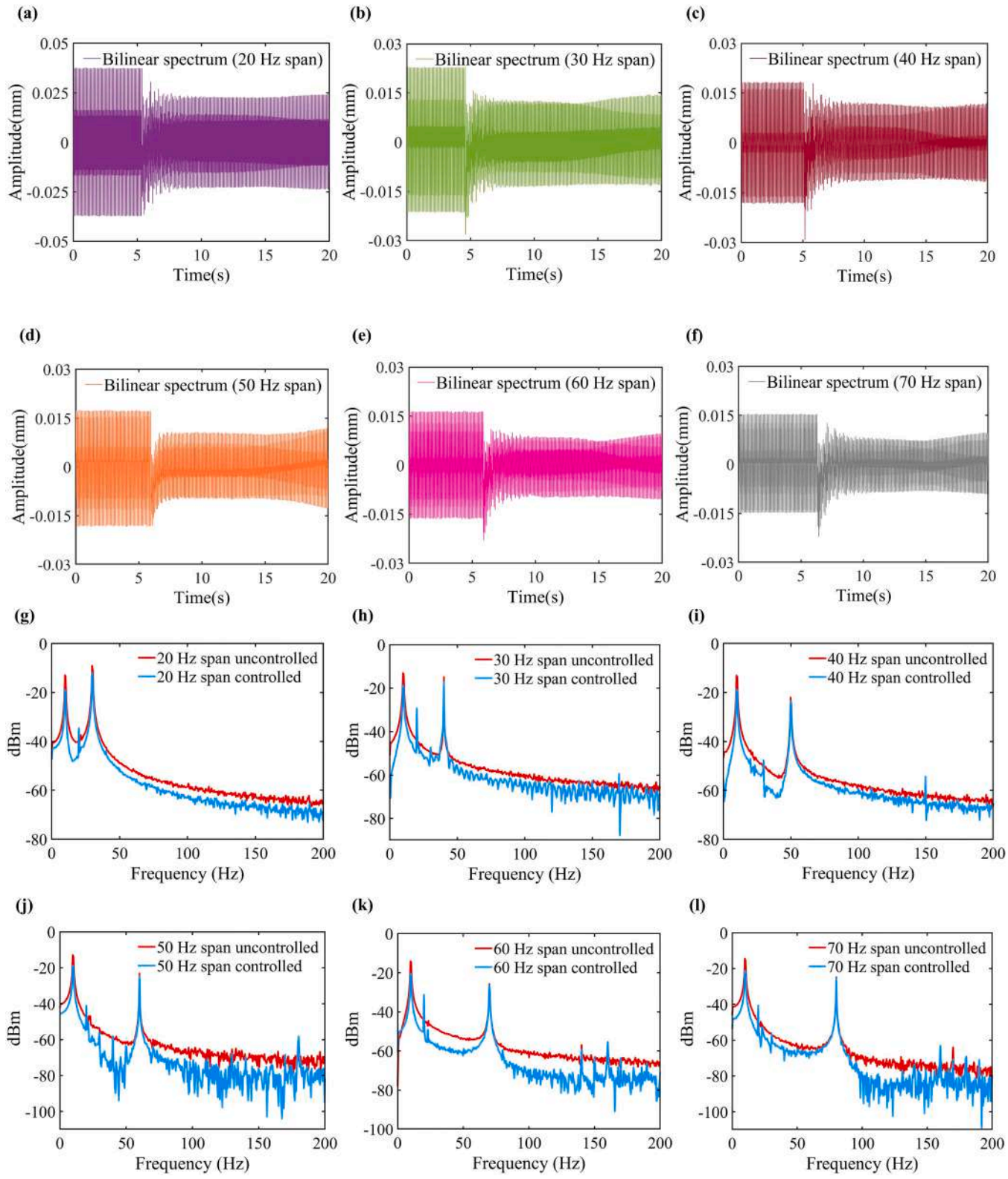

Fig. 12. Experimental results of active control of bilinear spectral vibration, Fig(a) to (l) are time and frequency domain diagram before and after controlling the bilinear spectral span.

each single-line spectrum, and a broadband suppression effect was realized in the medium frequency range. For the disturbances characterized by narrowband spectra, a vibration control effectiveness exceeding 10 dB was achieved in the narrowband range, and similarly, broadband suppression was realized in the medium frequency range.

4.2. Experiment of active control of piezoelectric cantilever vibration

An experimental investigation into active control of multiline spectra and narrowband vibration in high-rigidity piezoelectric cantilever beam structures was conducted. This study segmented the problem to examine

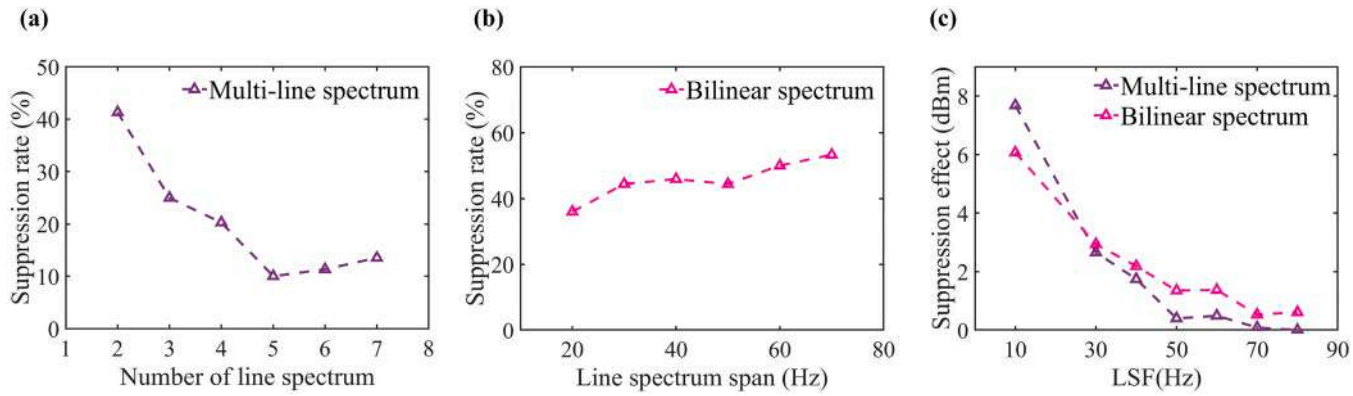

Fig. 13. (a) Effect of number of line spectra on vibration suppression rate, (b) Effect of line spectrum span on vibration suppression rate, (c) Effect of the single line spectral frequency on the vibration suppression.

the effects of various parameters: the number of lines in the multiline spectra of the excitation perturbation signals, their respective spans, and the center frequency and widths of the narrowband spectra. These parameters were analysed for their influence on the active control characteristics of high-rigidity piezoelectric cantilever beams.

The experiment utilized a PXI data acquisition system, with both the acquisition card and output card employing bus modules. The bus provided clock, trigger, and data communication, with a bandwidth of 4 GB/s. The system integrated a processor that ran a Linux Real-Time operating system, with timing cycles precise to the microsecond level. The measured average closed-loop control error was less than 10 μs. The acquisition card was configured for timed data collection at 1 ms intervals, and data was read point-by-point. The retrieved data was transmitted via a triggered queue to the closed-loop control algorithm cycle. Once the closed-loop computation was completed, the calculated result data was sent to the output module, which triggered the output module to send the output. Therefore, two triggered queues were employed, with both the algorithm step size and sampling period set to 1 ms. The actual time for a single state collection and feedback operation ranged from 200 to 300 μs. The design architecture diagram of the acquisition-closed loop operation-feedback system was shown in Fig. 10.

In the conducted experiments, the primary and secondary physical channels of the RU-FxLMS algorithm corresponded to actual components, including the piezoelectric cantilever beam structure, signal generator, signal collector, and power amplifier. In the implemented algorithm, the actual channel was substituted by the theoretical channel model, meaning that the analogue filter transfer functions for the primary and secondary channels within the control system were set to 1. Furthermore, the estimation of the secondary channel was refined by integrating random white noise as the training signal for compensation purposes.

4.2.1. *Multiline spectral vibration control experiment*

A simulated multiline spectral signal was generated by the host computer to drive the shaker, which in turn stimulated vibration of the cantilever beam. The frequencies of the simple harmonic signals were set at 10, 30, 40, 50, 60, 70, and 80 Hz. In the initial set of experiments, a vibration input signal comprising a double-line spectrum was established by superimposing a 10 Hz signal onto a 30 Hz base. This pattern was continued for subsequent experimental groups by incrementally superimposing additional single-line spectra. The number of features in the multiline spectrum was controlled to verify the active control characteristics of the piezoelectric cantilever beam vibration. The experimental results before and after implementation of control are depicted in Fig. 11.

As shown in Fig. 11, the experimental results indicated that with an increasing number of spectral lines, the overall vibration control effectiveness correspondingly decreased. Furthermore, the results demonstrated that an increase in the frequency of the single-line spectra led to a decline in the control effectiveness of that single-line spectrum.

A computer was utilized to simulate a double-line spectral signal, which activated the shaker and induced vibration of the cantilever beam. The input signals employed for double-line spectral vibration had the span of different frequencies. The eigenfrequency ranges of the two single-line spectra were adjusted to experimentally validate the active control capabilities for piezoelectric cantilever vibration. The comparative results before and after implementation of control are presented in Fig. 12.

As shown in Fig. 12, the experimental outcomes indicated that the extent of the frequency span between the two single-line spectra had a

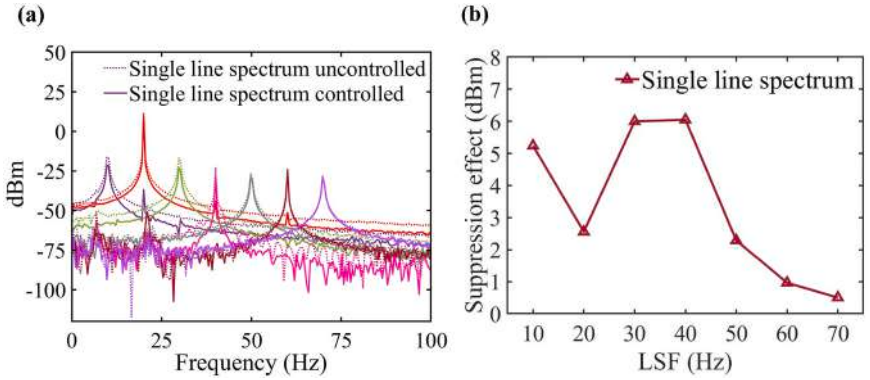

Fig. 14. Experimental results of vibration control of single line spectrum, (a) Frequency domain diagram before and after control, (b) Effect of the single line spectral frequency on the vibration suppression.

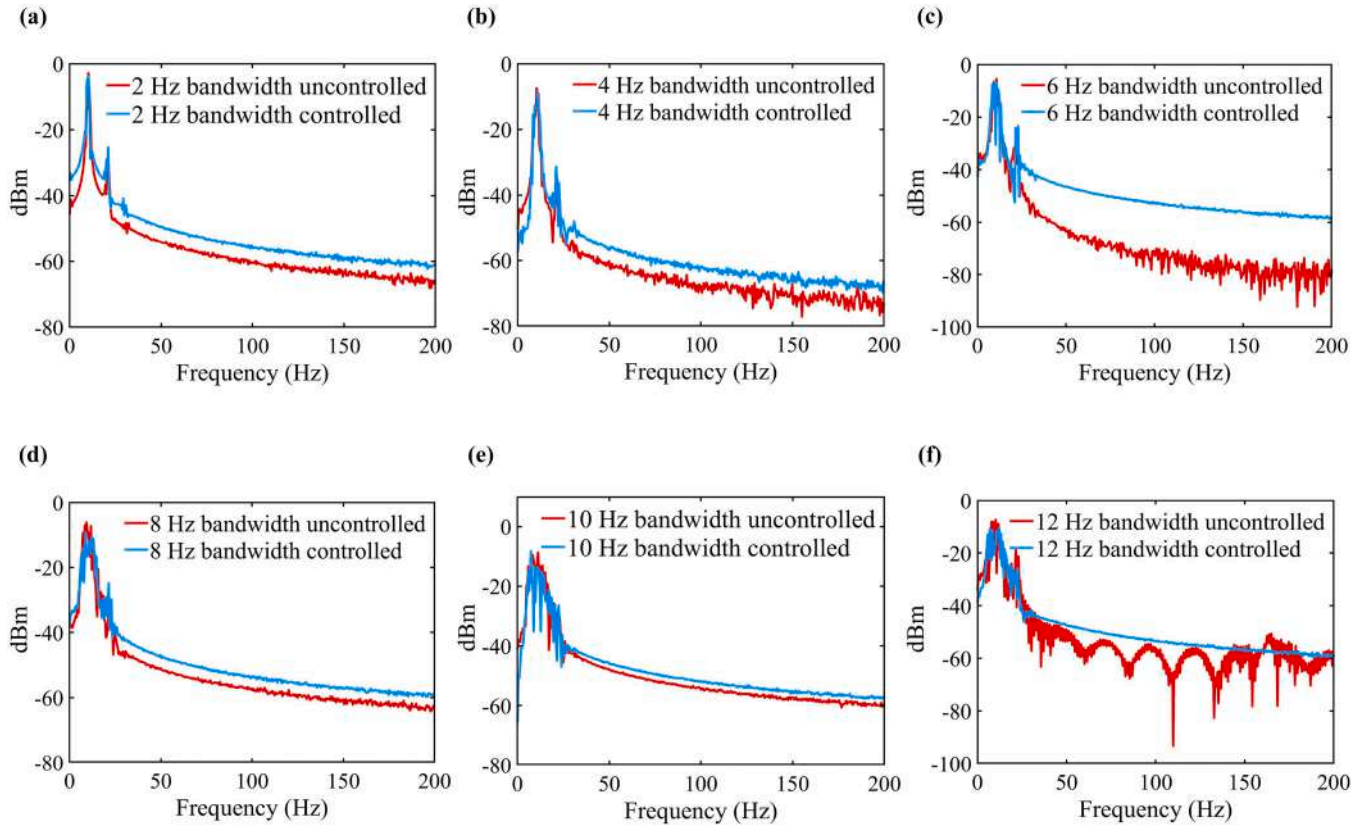

Fig. 15. Results of active control of narrowband spectral vibration with different bandwidths, Fig(a) to (f) are Frequency domain plots before and after vibration control at different bandwidths.

negligible effect on the overall vibration control efficacy. Nonetheless, as the frequency of the double-line spectra increased, the control effectiveness for the double-line spectrum deteriorated.

The control experiments conducted on multiline and double-line spectra facilitated the extraction of influential factors, which included the number of line spectra, the span of the line spectra, and the line spectral frequency (LSF). The experimental data were collated and are illustrated in Fig. 13.

As illustrated in Fig. 13(a), the vibration suppression rate was approximately 40 % when double-line spectra were exclusively present. As the number of line spectra increased, the suppression rate markedly decreased. The suppression rate approached an approximate value of 10 % when the number of line spectra reached five. As demonstrated in Fig. 13(b), an increase in the frequency span between two single-line spectra was associated with a modest increase in the vibration suppression rate, which generally stabilized at approximately 50 %. As indicated in Fig. 13(c), the single eigenfrequency within the multiline spectrum and the double-line spectrum were extracted and analysed separately. The suppression effect deteriorated with increasing frequency of the single-line spectrum. Furthermore, the trend of the degradation in the suppression capability for the multiline spectrum became more pronounced as the eigenfrequency increased. Overall, the presence of a brief time delay in the actual physical channel led to the finding that signals with a higher frequency incurred bigger phase and amplitude errors due to the time delay, which consequently impacted the control efficacy.

To further examine the control effect and influencing factors for the high-rigidity cantilever beam actuated by a piezoelectric device under a single-line spectral perturbation when employing the control strategy presented in this study, vibration control experiments were conducted. External excitations with frequencies of 10, 20, 30, 40, 50, 60, and 70 Hz were individually applied, and the outcomes of each experimental set were compiled, as depicted in Fig. 14.

As illustrated in Fig. 14, the vibration control effect was observed to exceed 2 dB for single-line spectral frequencies at or below 50 Hz. However, when the frequency exceeded 50 Hz, the vibration suppression rate rapidly decreased to less than 1 dB. The vibrational effects at 20 Hz were slightly less favourable than the control results obtained for the other low frequency spectral lines, and this divergence was attributed to the influence of the bolts and ribs employed in the mounting of the cantilever beam structure. The inherent frequency of the structure was identified to be approximately 20 Hz, which resulted in the control efforts for forced vibration near this frequency transitioning into management of the structural resonance.

4.2.2. Narrowband spectral vibration control experiment

The host computer generated an analogue, narrowband signal that activated the shaker and induced vibration of the cantilever beam. The center frequency was set at 10 Hz, and the span for the narrowband spectral vibration input signal was established as different frequencies. An experimental verification of the active control characteristics of the piezoelectric cantilever beam vibration for the narrowband spectrum was conducted. The results before and after control implementation are presented in Fig. 15.

As shown in Fig. 15, the experimental results indicated an enhancement in the vibration control effectiveness within the characteristic band as the width of the narrowband spectrum increased, whereas the vibration amplitude within the noncharacteristic band increased.

The host computer generated an analogue narrowband signal that drove the shaker to induce vibration of the cantilever beam. The span was set to 4 Hz, and the narrowband spectral vibration input signal had different center frequency. The center frequency of the narrowband spectrum was controlled to experimentally verify the active control

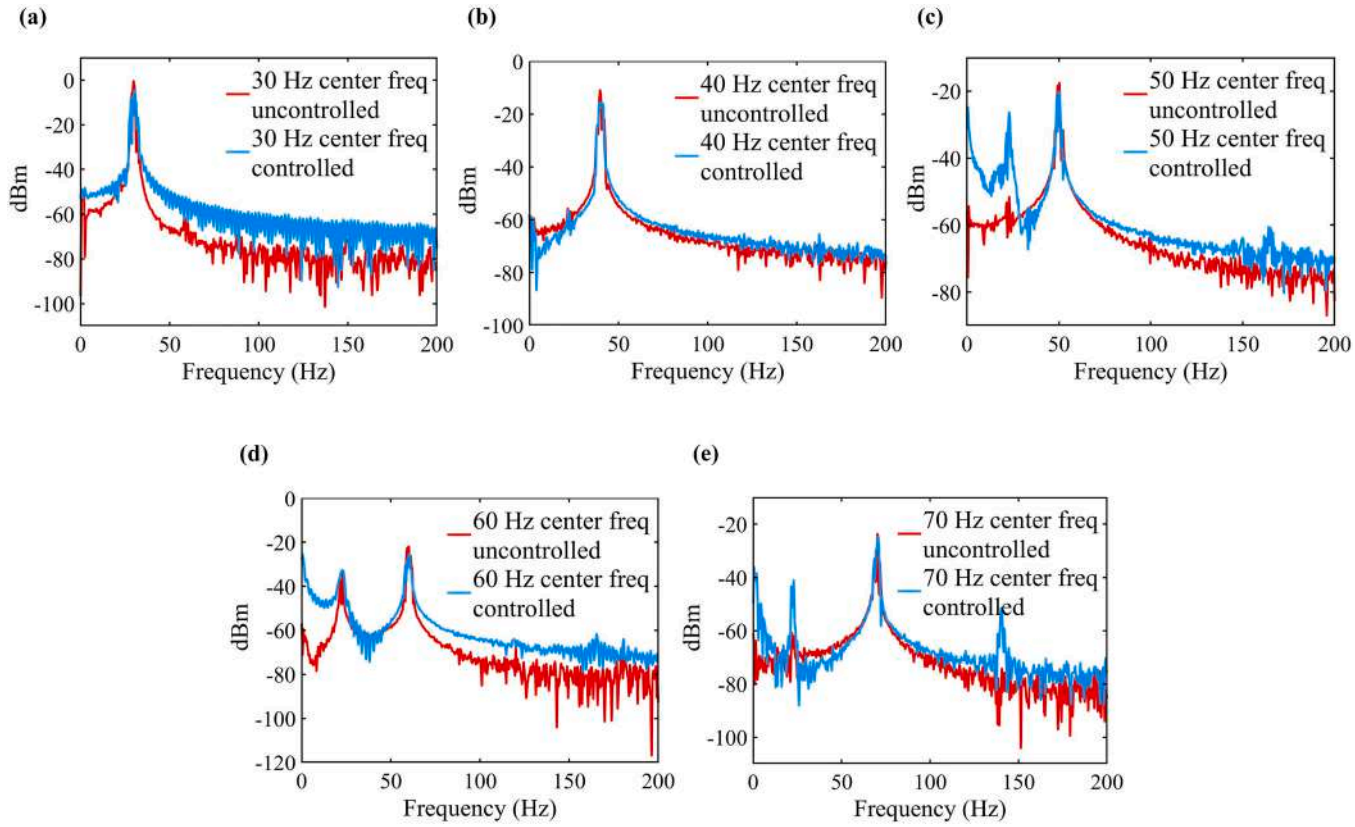

Fig. 16. Results of active control of narrowband spectral vibration with different center frequency, Fig(a) to (e) are Frequency domain plots before and after vibration control at different center frequency.

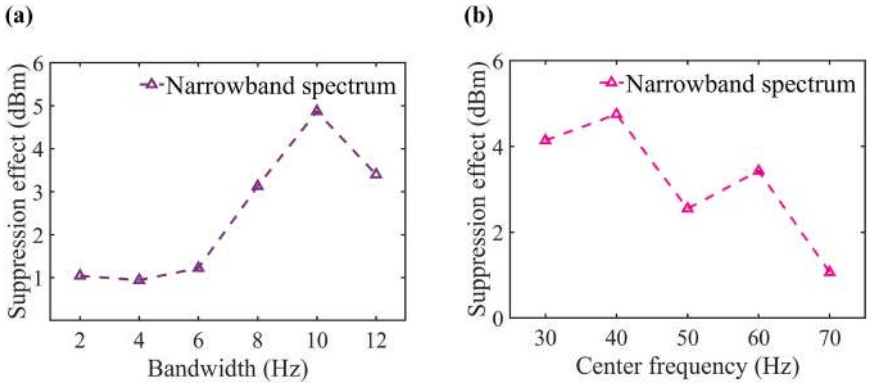

Fig. 17. (a) Effect of narrow band spectral width on vibration suppression, (b) Effect of the center frequency of the narrow band spectrum on the vibration suppression.

characteristics for piezoelectric cantilever vibration. The pre- and post-control experimental results are presented in Fig. 16.

As illustrated in Fig. 16, the experimental results indicated that the vibration control efficacy within the characteristic band diminished with increasing center frequency of the narrowband spectrum, while the vibration amplitude for the noncharacteristic band increased.

In the control experiments of the narrowband spectrum, the bandwidth and center frequency were identified as influencing factors. The data were collated and are presented in Fig. 17.

As depicted in Fig. 17(a), when the bandwidth was narrow, the suppression effect on the characteristic band vibration was approximately 1 dBm. An increase in the suppression effect was observed with increasing bandwidth. Fig. 17(b) illustrates that when the center frequency of the narrowband spectrum was low, the vibration suppression effect within the characteristic band was approximately 4 dBm. With an increase in the center frequency, a notable reduction in the suppression effect was observed. Overall, the presence of minor time delays within the actual physical channel led to inaccuracies in the algorithm tracking of the characteristic frequency bands of narrowband signals. This, in turn, caused the piezoelectric actuator to operate outside the characteristic frequency bands, resulting in suppression of vibration within the narrowband range and a slight amplification of vibration outside the narrowband range.

4.3. *Effectiveness analysis of the RU-FxLMS algorithm*

To further ascertain the efficacy of the control strategy within the low frequency band for suppression of vibration under multiline spectra,

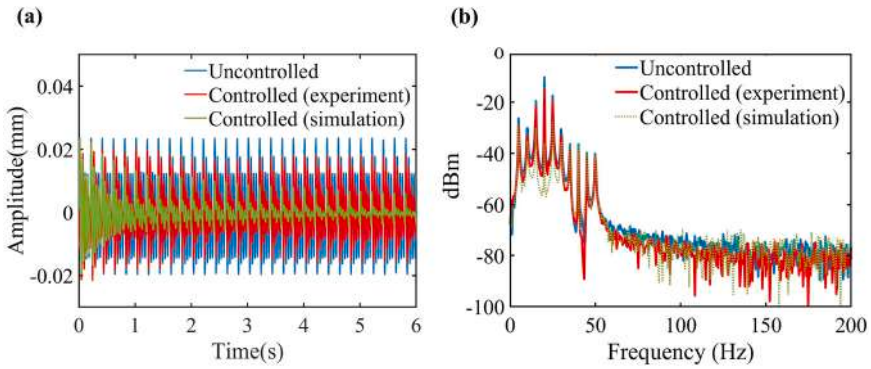

Fig. 18. Results of vibration control of multiline spectral vibration, (a) Time domain diagram before and after control, (b) Frequency domain diagram before and after control.

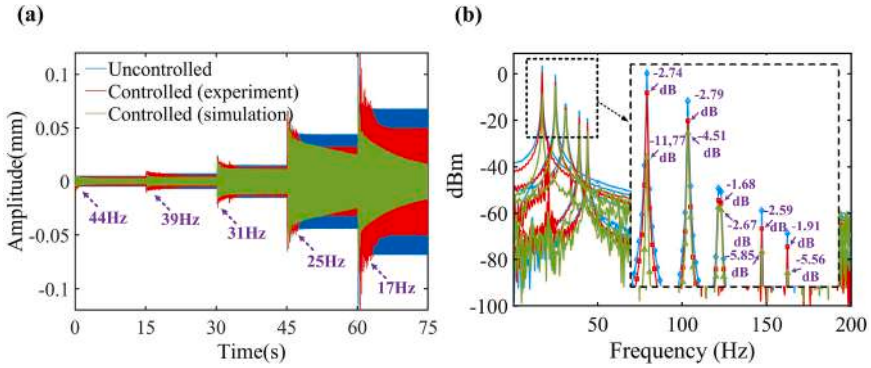

Fig. 19. Results of vibration control of frequency-hopping vibration (a) Time domain diagram before and after control, (b) Frequency domain diagram before and after control.

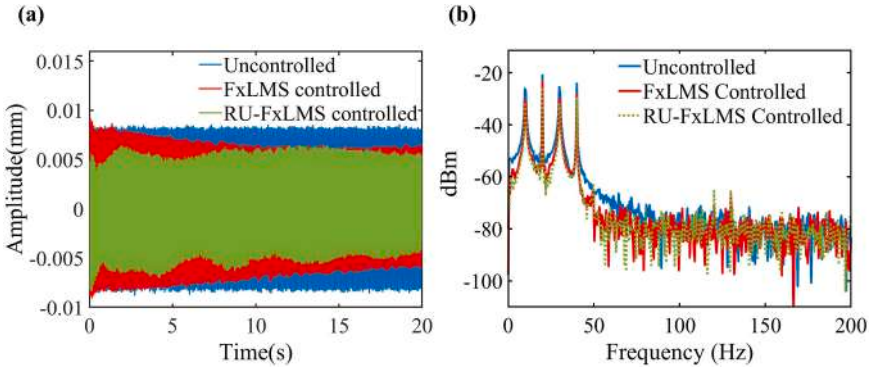

Fig. 20. Experimental results of vibration control of multiline spectral vibration (a) Time domain diagram before and after control, (b) Frequency domain diagram before and after control.

ten-line spectral vibration control and frequency-hopping tracking control simulation and experiment were conducted within the frequency range of 0–50 Hz. The consistency between simulation and experimental results was validated through the implementation of closed-loop control for the two prevalent vibration conditions commonly encountered in engineering. The results of these simulations and experiments are presented in Fig. 18 and Fig. 19.

As depicted in Fig. 18 and Fig. 19, within the low frequency band ranging from 0 to 50 Hz, the control strategy could effectively manage up to ten-line spectra and frequency-hopping spectra. In the simulations and experiments conducted under two distinct operational conditions, the time-domain results indicated that the control performance in the simulation surpassed that of the experiment, albeit with a slower convergence rate. The physical channels in the experiment exhibited inherent time delays, which marginally compromised the control effectiveness and the simulation incorporated an additional primary channel model and variable step-size control strategy, which contributed to the slower convergence. This outcome was consistent with expectations. The trends observed in both the simulation and experimental results were rational, thereby validating the efficacy of the control algorithm.

To further investigate the superiority of the improved algorithm, closed-loop control experiments were conducted under multiline spectral vibration conditions. Both the conventional and the improved FxLMS algorithms were employed in these experiments. The experimental results are presented in Fig. 20.

As shown in Fig. 20, the presence of the "reset" module allowed the feedback signal to be periodically reset to a specified amplitude. This

feature enabled the improved method to effectively control the vibrations rapidly. In Fig. 20(a), the adjustment time was significantly reduced compared to traditional control methods. The nonlinearity during the moment of resetting caused minor fluctuations in the controlled amplitude during the initial stages of control, which subsequently stabilized. Due to the presence of the " uniformization " module, the feedback signal was able to stabilize the amplitude at the maximum output voltage of the actuator while maintaining the frequency and phase unchanged, resulting in improved control performance. In Fig. 20 (b), the suppression effect on each spectral line was higher compared to traditional control methods. This validated that the improved RU-FxLMS algorithm exhibited enhanced control capability in the low-frequency range.

5. Conclusion

This study investigated the active control characteristics of large-section and high-rigidity piezoelectric cantilever beams under multiline and narrowband vibration. The traditional LMS algorithm was enhanced, and a RU-FxLMS controller was designed by identifying and compensating the secondary channel online, as well as by constructing a reset & uniformization module to address the instability in vibration signals collected by sensors, thereby maximizing the output capability and ensuring the smoothness of the output signal. The intrinsic equations of a high-rigidity piezoelectric cantilever beam, which incorporated feedback, control and observation, were integrated. The equations enabled extraction of the state at any point along the beam at any given moment before and after vibration control. Additionally, active control simulations pertaining to the vibration of a piezoelectric cantilever beam were conducted. The tracking efficiency, convergence, and nonlinear characteristics of the algorithm were verified and analysed. In the case of multiline spectral disturbances, the system achieved a suppression effect that varied between 4 and 13 dBm for each individual line spectrum, while a broadband suppression effect was realized within the high frequency band. Regarding narrowband spectral interference, the system attained a significant suppression effect over the entire frequency range, with a notable 10 dBm suppression effect being realized in the characteristic narrowband spectrum.

Ultimately, active vibration control experiments were conducted on piezoelectric cantilever beams. The effects of the multiline spectral number, span, and frequency and the central frequency and width of narrowband spectra on the active vibration control properties of high-rigidity piezoelectric cantilever beams were investigated. The experiments revealed the following: (1) In the case of multiline spectral disturbances, the number of line spectra exerted a larger influence on the vibration suppression rate, whereas the span between line spectra had a lesser effect, and effective vibration control was realized within the low frequency range from 0–50 Hz. (2) With respect to narrowband spectrum disturbances, the center frequency of the narrowband spectrum had a more significant impact on the vibration suppression effectiveness, whereas the width of the narrowband spectrum influenced the suppression within a specific bandwidth. (3) The results of vibration control in multiline spectra and frequency-hopping vibration demonstrated that the trends in the simulations were consistent with those in the experiments. This consistency validated the accuracy of the constitutive modelling of the piezoelectric cantilever beam and confirmed the efficacy of the proposed improved algorithm. This provides a novel approach for the active control of multilinear and nonlinear vibration in the low frequency range for high-rigidity structures.

CRediT authorship contribution statement

Xin Lan: Writing – review & editing, Methodology, Data curation. **Weikai Shi:** Writing – review & editing, Visualization, Data curation. **Liwu Liu:** Writing – review & editing, Investigation, Conceptualization. **YANJU LIU:** Writing – review & editing, Investigation, Conceptualization. **Pengxiang Zhao:** Writing – review & editing, Visualization, Data curation. **Jianlong Gao:** Writing – review & editing, Visualization, Data curation. **Jinsong Leng:** Writing – review & editing, Supervision, Investigation. **Xudong Zhang:** Writing – review & editing, Writing – original draft, Visualization, Investigation, Formal analysis, Conceptualization.

Declaration of Competing Interest

We declare that we do not have any commercial or associative interest that represents a conflict of interest in connection with the work submitted.

Acknowledgements

The author of this article would like to express heartfelt gratitude to the following experts for their invaluable support: Academician Leng for providing the instruments and equipment used in the experiments, Professor Lan for guiding the experimental work, and Professor Liu for offering suggestions on the theoretical modeling. Sincere thanks to all of them!

Data Availability

Data will be made available on request.

References

[1] Hashemi A, Jang J, Hosseini-Hashemi S. Smart active vibration control system of a rotary structure using piezoelectric materials. Sensors 2022;22:1–15.
[2] Zhou MD, Liu W, Tang LL, Yao Z, Wen ZQ, Liang B, et al. Multidimensional vibration suppression method with piezoelectric control for wind tunnel models. Sensors 2019;19(18):3998.
[3] Luo HT, Li HD, Wu XY, Liu GM, Zhang W. Dynamic modeling and active vibration control of piezoelectric laminated structure based on macrofiber composite. Struct Control Health Monit 2024;2024:8826434.
[4] Zhang H, Sun W, Luo HT, Zhang RF. Modeling and active control of geometrically nonlinear vibration of composite laminates with macro fiber composite. Compos Struct 2023;321:117292.
[5] Przybylski J, Kulinski K. Nonlinear vibrations of a sandwich piezo-beam system under piezoelectric actuation. Nonlinear Dyn 2022;109(2):689–706.
[6] Raza A, Rimasauskiene R, Jurenas V, Mahato S. Experimental investigation of vibration amplitude control in additive manufactured PLA and PLA composite structures with MFC actuator. Eng Struct 2023;294:116802.
[7] Salem MAM, Kassem M, Amin MS, Farag HM, Osman A. Energy-based optimal placement of piezoelectric actuator on smart thin plate. J Vib Eng Technol 2023;12 (2):1813–30.
[8] Jeong UC, Kim JS, Kim YD, Oh JE. Reduction of radiated exterior noise from the flexible vibrating plate of a rectangular enclosure using multi-channel active control. Appl Acoust 2016;105:45–54.
[9] Wang XM, Zhou WY, Wu ZG, Zhang XH. Integrated design of laminated composite structures with piezocomposite actuators for active shape control. Compos Struct 2019;215:166–77.
[10] Chen FL, Liu LW, Li QY, Epaarachchi J, Leng JS, Liu YJ. Experimental and theoretical analysis of a smart transmission mechanism system. Smart Mater Struct 2018;27(9):095022.
[11] Zhang Q, Li CD, Zhang JT, Zhang JH. Smooth adaptive sliding mode vibration control of a flexible parallel manipulator with multiple smart linkages in modal space. J Sound Vib 2017;411:1–19.
[12] Liu T, Liu CC, Zhang Z. Adaptive active vibration control for composite laminated plate: theory and experiments. Mech Syst Signal Process 2024;206:110876.
[13] Shi F, Cao HR, Zhang XW, Chen XF. A chatter mitigation technique in milling based on H_∞-ADDPMS and piezoelectric stack actuators. Int J Adv Manuf Technol 2019; 101(9-12):2233–48.
[14] Ripamonti F, Giampà A, Giona R, Liu L, Corradi R. Numerical and experimental study of an active control logic for modifying the acoustic performance of single-layer panels. J Sound Vib 2022;520:116608.
[15] Li C, Shen L, Shao J, Fang JW. Simulation and experiment of active vibration control based on flexible piezoelectric MFC composed of PZT and PI layer. Polymers 2023;15(8):1819.
[16] Bhattacharyya S, Ghosh AD, Basu B. Design of an active compliant liquid column damper by LQR and wavelet linear quadratic regulator control strategies. Struct Control Health Monit 2018;25(12):e2265.
[17] Wan HP, Ma Q, Dong GS, Luo YZ, Ni YQ. Data-driven model reduction approach for active vibration control of cable-strut structures. Eng Struct 2024;302:117434.
[18] Saint Martin LB, Mendes RU, Cavalca KL. Electromagnetic actuators for controlling flexible cantilever beams. Struct Control Health Monit 2018;25(1):e2043.

[19] Zhang H, Sun W, Luo HT, Zhang RF. Active vibration control of composite laminates with MFC based on PID-LQR hybrid controller. Mech Adv Mater Struct 2023.
[20] Zhai XH, Luo YJ, Xie SL, Xu ML, Zhang XN. Active vibration control of loop antenna structure. Int J Appl Electro Mech 2019;59(3):951–8.
[21] Boz U, Basdogan I. IIR filtering based adaptive active vibration control methodology with online secondary path modeling using PZT actuators. Smart Mater Struct 2015;24(12):125001.
[22] Wu HC, Yang TS, Xiao WH, Wang XL, Wang WY. Online active vibration control for the magnetic suspension rotor using least mean square and polynomial fitting. Nonlinear Dyn 2024;112(9):7029–41.
[23] Ma GL, Wang PP, Chen LQ, Brighton NC, Anish M. Suspension nonlinear analysis and VSS-LMS adaptive filtering control of satellite borne flexible structure. Nonlinear Dyn 2024;112(5):3679–93.
[24] Tian J, Guo Q, Shi G. Laminated piezoelectric beam element for dynamic analysis of piezolaminated smart beams and GA-based LQR active vibration control. Compos Struct 2020;252:112480.
[25] Pu YX, Zhou HL, Meng Z. Multi-channel adaptive active vibration control of piezoelectric smart plate with online secondary path modelling using PZT patches. Mech Syst Signal Process 2019;120:166–79.
[26] Qiu ZC, Wang XF, Zhang XM, Liu JG. A novel vibration measurement and active control method for a hinged flexible two-connected piezoelectric plate. Mech Syst Signal Process 2018;107:357–95.
[27] Wang M, Fang X, Wang YY, Ding JH, Sun Y, Luo J, et al. A dual-loop active vibration control technology with an RBF-RLS adaptive algorithm. Mech Syst Signal Process 2023;191:110079.
[28] Xie LB, Qiu ZC, Zhang XM. Vibration control of a flexible clamped-clamped plate based on an improved FULMS algorithm and laser displacement measurement. Mech Syst Signal Process 2016;75:209–27.
[29] Qiu ZC, Han JD, Zhang XM, Wang YC, Wu ZW. Active vibration control of a flexible beam using a non-collocated acceleration sensor and piezoelectric patch actuator. J Sound Vib 2009;326(3-5):438–55.
[30] Yang TP, Li PQ, Li QP, Li ZR. Active suspension control strategy for vehicles based on road surface recognition. Nonlinear Dyn 2024;112(13):11043–65.
[31] Zhang J, Hu XM, Wu JY, Lim YM, Gong SH, Liu RW. Shear behavior of headed stud connectors in steel-MPC based high strength concrete composite beams. Eng Struct 2021;249:113302.
[32] Li F, Peng HJ, Song XS, Liu JG, Tan SJ, Ju ZJ. A physics-guided coordinated distributed MPC method for shape control of an antenna reflector. IEEE Trans Cyber 2022;52(10):10263–75.
[33] Feng XD, Fan YB, Peng HJ, Chen Y, Zheng YW. Optimal active vibration control of tensegrity structures using fast model predictive control strategy. Struct Control Health Monit 2023;2023:2076738.
[34] Meng D, Xia PQ, Song LS. MIMOMH feed-forward adaptive vibration control of helicopter fuselage by using piezoelectric stack actuators. J Vib Control 2018;24 (23):5534–45.
[35] Xie CH, Wu Y, Liu ZS. Modeling and active vibration control of lattice grid beam with piezoelectric fiber composite using fractional order PD$^{\mu}$ algorithm. Compos Struct 2018;198:126–34.
[36] Xu LL, Yu YY, Cui YL. Active vibration control for seismic excited building structures under actuator saturation, measurement stochastic noise and quantisation. Eng Struct 2018;156:1–11.
[37] Zang J, Ren HM, Song XY, Zhang Z, Zhang YW, Chen LQ. Vibration control of interconnected composite beams: Dynamical analysis and experimental validations. Mech Syst Signal Process 2024;208:111008.
[38] Jokar H, Vatankhah R, Mahzoon M. Active vibration control of horizontal-axis wind turbine blades using disturbance observer-based boundary control approach. Eng Struct 2023;275:115323.
[39] Wang YG, Kang Z, Zhang XP. A velocity field level set method for topology optimization of piezoelectric layer on the plate with active vibration control. Mech Adv Mater Struct 2023;30(7):1326–39.
[40] Zhang XP, Takezawa A, Kang Z. Topology optimization of piezoelectric smart structures for minimum energy consumption under active control. Struct Multidiscipl Optim 2018;58(1):185–99.
[41] Presas A, Luo YY, Wang ZW, Valentin D, Egusquiza M. A review of PZT patches applications in submerged systems. Sensors 2018;18(7):2251.
[42] Ma GL, Xu ML, Liu T, Luo YJ. The multi-body analysis and vibration control of the second-order mode of a hoop flexible structure. Acta Mech 2019;230(4):1377–86.
[43] Xu PL, Lan X, Zeng CJ, Zhang XD, Liu YJ, Leng JS. Dynamic characteristics and active vibration control effect for shape memory polymer composites. Compos Struct 2023;322:117327.
[44] Gao H, Wang H, Li J, Lang TY, Gao WJ, Tao TY. Spacers combined with dampers for the wake-induced vibration mitigation of two parallel hanger cables. Eng Struct 2024;304:117590.
[45] Tso MH, Yuan J, Wong WO. Design and experimental study of a hybrid vibration absorber for global vibration control. Eng Struct 2013;56:1058–69.
[46] Yang MG, Hu RK, Meng DL, Zhang HJ. A novel Horizontal Bidirectional Hybrid Damping System (HBHDS) for multi-level vibration control of long-span bridges: a theoretical study. Eng Struct 2024;305:117693.